# Comparison of Shapes of Two-Dimensional Figures with the Use of Morphological Spectra and EMD Metrics[1]

## Yu. V. Vizilter and S. V. Sidyakin

*State Research Institute of Aviation Systems, ul. Viktorenko 7, Moscow, 125319 Russia*
*e-mail: viz@gosniias.ru, sersid@bk.ru*

**Abstract**—It is shown that the problems of real-time classification of two-dimensional figures and binary images can be successfully solved on the basis of comparison of discrete–continuous morphological pattern spectra with the use of the EMD-L[1] metric.

## INTRODUCTION

In [1], Maragos proposed a method for describing flat figures and images by means of shape-size pattern spectra calculated on the basis of Serra's mathematical morphology [2]. In [3], we considered a computationally efficient algorithm for constructing morphological spectra of figures and images that is based on a continuous skeletal morphology [4]. This made it possible to apply morphological spectra in real-time machine vision systems; hence, the question of potential fields of application of these spectra has become topical.

Today, in most known practical applications, morphological spectra are used for texture analysis [5–7]. Examples of application of morphological spectra as descriptors of the shapes of objects in recognition problems are extremely rare. This is associated with two factors. First, efficient metrics for comparing spectra have not been proposed that would allow one to determine the membership of figures in one or other class of shapes. Second, the thickness distribution of a figure described by a pattern spectrum [1] is not informative enough to recognize the class of figures by this feature alone.

In this work, we experimentally show that the comparison of morphological spectra in recognition problems can be successfully carried out by means of Earth Mover's Distance (EMD) metrics [8]. In test problems, in most cases one can recognize classes of complex shapes solely on the basis of a comparison of morphological spectra. However, in real problems, along with samples that can be distinguished from their rich thickness features, uninformative samples (or samples

similar in terms of thickness) can be encountered; in this case, it is suggested that one use morphological spectra as an additional tool for recognizing figures by other methods.

## A DISCRETE MORPHOLOGICAL PATTERN SPECTRUM

The idea of calculating the morphological spectra of binary flat figures consists in the following. Assume figure $X$ and structuring element $B$ that includes the origin $(0, 0)$ in plane $P$ of the figure. Introduce the concept of parametrically scalable element $B(r)$, which has the shape of figure $B$:

$$B(r) = \{rb \,|\, b \in B\}, \quad r \geq 0, \quad b = (x_b, y_b) \in P,$$

where $r$ is the size of the structuring element and $b$ is a point with coordinates $(x_b, y_b)$ that belongs to $B$. Consider a binary image of $X \subseteq P$. Define morphological (pattern) spectrum $PS$ of $X$ with respect to $B \subseteq P$ as a function:

$$PS_{X,B}(r) = -\frac{\partial S(X \circ B(r))}{\partial r}, \quad r \geq 0; \qquad (1)$$

$$PS_{X,B}(-r) = \frac{\partial S(X \bullet B(r))}{\partial r}, \quad r < 0, \qquad (2)$$

where $S(X \circ B(r))$ is the area of opening of figure $X$ by element $B$ and $S(X \bullet B(r))$ is the area of closing figure $X$ by element $B$. Formulas (1) and (2) define the spectrum for the positive and negative parts of the $r$ axis, respectively. This means that $S(X \circ B(r))$ is a measure of $B(r)$ in $X$. Figure 1 shows the morphological spectrum of objects on the image of $X$ with a circular structuring element and the steps of its morphological processing. Since it is inconvenient to perform calcula-
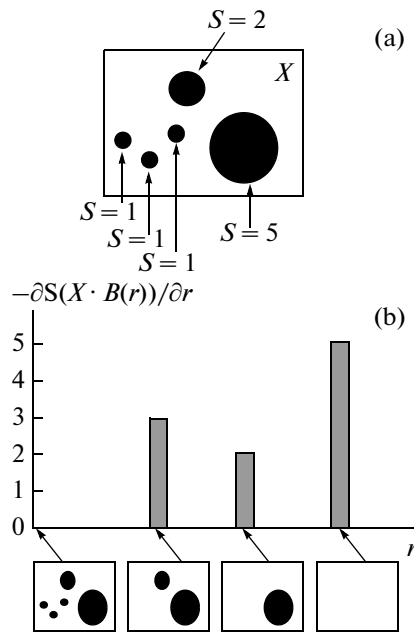
---

**Fig. 1.** Morphological spectrum of objects on image $X$ with a disc structuring element and stages of its morphological processing: (a) original image $X$ with disks with area $S$ and (b) monotonic decrease in complexity.

tions with derivatives in (1) and (2), in practice one introduces a discrete morphological spectrum:

$$PS_{X, B}(r) = -\frac{S(X \circ B(r_i)) - S(X \circ B(r_{i+1}))}{r_i - r_{i+1}} \quad (1')$$

for $r_i \leq 0$ and

$$PS_{X, B, \Delta r}(r_i) = \frac{S(X \bullet B(-r_i)) - S(X \bullet B(-r_{i+1}))}{r_{i+1} - r_i}, \quad (2')$$

for $r_i < 0$,

where $r_i = i\Delta r$, $i \in Z$ and $\Delta r$ is a scale sampling step.

In this paper, we propose using the EMD metric for comparing morphological pattern spectra.

## MD METRIC AND A HISTOGRAM COMPARISON PROBLEM

In [8], the notion was introduced of EMD metrics, which are used for comparing "histogram-like" object descriptions represented by a finite set (array) of pairs $\langle P_i, h_{Pi} \rangle$, where $P_i$ is the $i$th object of description and $h_{Pi}$ is its weight (significance in the description). It is assumed that the object belongs to set $O$ and the weights are nonnegative real numbers. If a certain base (Earth) metric $d_E$ is known that allows one to pairwise compare objects from $O$, then one can define an EMD metric $d_{EMD}$ on the basis of this metric for comparing two histogram-like descriptions $P$ and $Q$:

$$d_{EMD}(P, Q) = \min_{\{h_{ij}\}} \sum_{j=1}^{m} \sum_{o=1}^{n} h_{ij} d_E(P_i, Q_i); \quad (3)$$
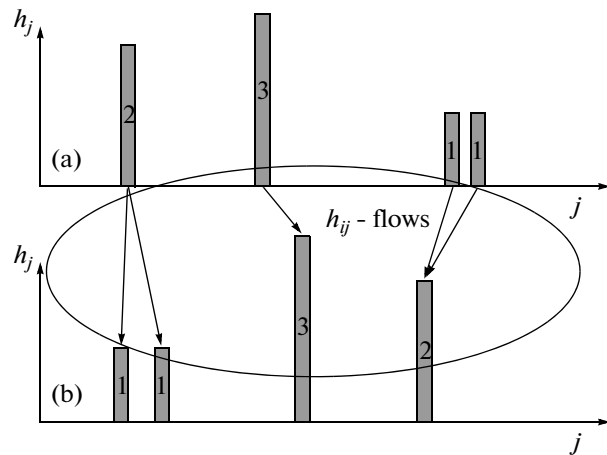


**Fig. 2.** Optimization of transportation of weights from (a) a source, a $P$ histogram, to (b) a receiver, a $Q$ histogram.

$$\sum_{i=1}^{n} h_{Pi} = 1; \quad \sum_{j=1}^{m} h_{Qj} = 1; \quad \sum_{j=1}^{m} \sum_{i=1}^{n} h_{ij} = 1;$$

$$\forall i, j : h_{ij} \geq 0; \quad h_{Pi} = \sum_{j=1}^{m} h_{ij}; \quad h_{Qj} = \sum_{i=1}^{n} h_{ij},$$

where $h_{ij}$ are flows between objects $P_i$ and $Q_j$; $n$ is the number of objects $P_i$ in description $P$; $m$ is the number of objects $Q_j$ in description $Q$; and $h_{Pi}$ and $h_{Qj}$ are the weights of objects in descriptions $P$ and $Q$, respectively.

When objects $P_i$ and $Q_j$ are given by the values $X_i$ and $Y_j$ of some random variables $X$ and $Y$, respectively, and descriptions $P$ and $Q$ represent discrete histograms of their distribution (for example, brightness histograms of a half-tone image), distance (3) turns out to be a particular case of the first-order ($s = 1$) Wasserstein distance [9] between probability densities $P(X)$ and $Q(Y)$ of random variables $X$ and $Y$:

$$W_s(P, Q) = (\inf E[d_E(X, Y)^s])^{1/s},$$

where the minimum of the mathematical expectation $E(\cdot)$ is taken over all possible pairs of values of random variables $X$ and $Y$. Note that the first-order Wasserstein distance is a particular case of the Kantorovich−Rubinstein distance on the metric space of Borel probability measures or the Monge−Kantorovich distance [10].

Thus, the EMD distance determines the minimum cost of the transformation of description $P_i$ to description $Q_i$. Here, it is assumed that every object from description $P_i$ should distribute all its "weight" to objects from description $Q$. In formula (3), the variables $h_{ij}$ represent a fraction of weight transported by object $P_i$ to object $Q_j$. The penalty for transporting this fraction of weight is taken to be equal to $d_E(P_i, Q_j)$: the closer objects $P_i$ and $Q_j$ in the sense of the base metric chosen, the smaller the penalty for transporting the weight of the object. In the general case, distance (3) is calculated by solving the so-called transport problem

by a linear programming method. Figure 2 illustrates the optimization of the transport of weights from the source (a $P$ histogram ($a$)) to the receiver (a $Q$ histogram ($b$)).

In a particular case in which the random variables are one-dimensional: $x \in R$, $y \in R$, histograms $P(x_i)$ and $Q(y_j)$ are one-dimensional discrete arrays. If the base metric on $R$ is an $L^1$ metric and $\sum_{j=1}^{m} Q(y_j) = \sum_{i=1}^{n} P(x_i)$, then, as is shown in [11], the EMD-$L^1$ distance can be calculated by the formula

$$d_{\text{EMD-L}^1}(P, Q) = \int_{-\infty}^{+\infty} |F(x) - G(x)| dx, \quad (3')$$

where $F(x)$ and $G(x)$ are the distribution functions for $P(x_i)$ and $Q(y_j)$:

$$F(x) = \int_{-\infty}^{x} P(t)dt \quad \text{and} \quad G(x) = \int_{-\infty}^{x} Q(t)dt.$$

Thus, on the basis of formula (3'), one can implement an efficient algorithm for calculating the EMD-$L^1$ distance between two one-dimensional histograms of fixed size in time linear with respect to the number of elements of the histogram.

As is shown below, the discrete morphological spectrum (1') and (2') is a histogram of a discrete thickness map of a binary image. Thus, one can apply the EMD-$L^1$ metric to compare the spectra of binary images.

## THICKNESS MAP AND ITS RELATION TO MORPHOLOGICAL SPECTRA

Assume binary figure $X$ that lies completely in a frame $K$: $X \subseteq K$. Denote by $X^{C(K)} = K \backslash X$ either a complement or the background of figure $X$ in the frame $K$. Figure $X$ can then be assigned a binary image $f_X(x, y)$:

$$f_X(x, y) = \begin{cases} 1, & \text{if} \quad p = (x, y) \in X; \\ 0, & \text{if} \quad p = (x, y) \in X^{C(K)}, \end{cases}$$

where $p$ is a point with coordinates $(x, y)$ in the frame.

Take a binary figure $B(q, r)$ with its center at point $q = (x, y) = B(q, 0)$ and scale parameter $r$ as a transportable and scalable element (in a particular case, this may be a disk).

A thickness map of a binary image $f_X(x, y)$ with structuring element $B$ is a real-valued image defined on frame $K$. The maximum size of the structuring element is recorded at each point of this image. Such structuring elements are completely inscribed in the figure or in its complement (in the latter case, the value of the dimensional parameter is assumed to be negative):

$$T_B(f_X) = t_{X, B}(x, y)$$

$$= \begin{cases} -\max_{r \in R}\{(x, y) \in B(q, r) \subseteq X^{C(K)}\} : (x, y) \in X^{C(K)}; \\ 0 : (x, y) \in \partial X = \partial X^{C(K)}; \\ \max_{r \in R}\{(x, y) \in B(q, r) \subseteq X\} : (x, y) \in X. \end{cases} \quad (4)$$

Let us establish a relation between thickness map (4) and the operations of opening and closing in Serra's binary morphology [2]:

$$X \circ B(r) = \{(x, y): t_{X, B}(x, y) \geq r\};$$

$$X \bullet B(r) = \{(x, y): t_{X, B}(x, y) \geq -r\}.$$

Define a function

$$\chi_{X, B}(x, y, r) = \begin{cases} 1 : t_{X, B}(x, y) \geq r; \\ 0 - \text{otherwise} \end{cases}$$

and, using this function, introduce a measure

$$\mu_{X, B}(r) = \|\chi_{X, B}(x, y, r)\|_{L^1}$$

$$= \iint \chi_{X, B}(x, y, r) dx dy.$$

Since

$$\mu_{X, B}(r) = \begin{cases} \|X \circ B(r)\|_{L^1} : r \geq 0; \\ \|X \bullet B(-r)\|_{L^1} : r < 0, \end{cases}$$

this measure allows one to give an alternative definition of the morphological spectrum:

$$PS_{X, B}(r) = -\frac{\partial \mu_{X, B}(r)}{\partial r}. \quad (5)$$

Thus, the morphological spectrum (1)−(2) is the distribution density of values of the thickness map $T_B(f_X)$.

Now, suppose that dimension parameter $r$ can take only discrete values from the set $RZ = \{r_i = i\Delta r, i \in Z\}$ with some $\Delta r > 0$. Since, for any frame $K$ of finite size, there exists an $r_{\max} = \max\{r : B(r) \subseteq K\}$, $r_{\max} < \infty$, it follows that, in fact, parameter $r$ can take values only from the set

$$RZ(K)$$

$$= \left\{ r_i = i\Delta r, i = -i_{\max}, \dots, i_{\max}; i_{\max} = \left\lfloor \frac{r_{\max}}{\Delta r} \right\rfloor \right\},$$
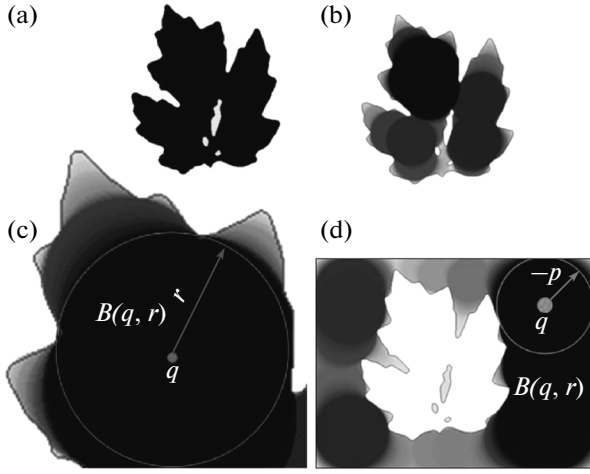
**Fig. 3.** Binary image and the discrete thickness maps of an object (foreground) and the background: (a) binary figure $X$, (b) expanded part of a real-valued image of a discrete thickness map for binary figure $X$ interpreted as an inverted half-tone image, (c) thickness map for binary figure $X$, and (d) thickness map for the background of figure $X$.

where $\lfloor r_{max}/\Delta r \rfloor$ is a maximum integer no greater than $r_{max}/\Delta r$. Such a set of dimensions generates a discrete thickness map (Fig. 3):

$$T_{B, \Delta r}(f_X) = t_{X, B, \Delta r}(x, y)$$

$$= \begin{cases} - \max_{r \in RZ(K)} \{(x, y) \in B(q, r) \subseteq X^{C(K)}\}: (x, y) \in X^{C(K)}; \\ 0: (x, y) \in \partial X = \partial X^{C(K)}; \\ \max_{r \in RZ(K)} \{(x, y) \in B(q, r) \subseteq X\}: (x, y) \in X. \end{cases} \quad (6)$$

The thickness map can be represented in a mosaic form [12]:

$$t_{X, B, \Delta r}(x, y) = \sum_{i = -i_{max}}^{i_{max}} r_i \chi_{X_i}(x, y),$$

and, hence, one can define a normalized histogram of a discrete thickness map:

$$H(t_{X, B, \Delta r}) = \left\{ \langle r_i, h_{X_i} \rangle : h_{X_i} = \frac{\iint \chi_{X_i}(x, y) dx dy}{S} \right\}, \quad (7)$$

$$i = -i_{max}, \dots, i_{max}.$$

*Proposition.* The discrete morphological spectrum (1')−(2') is proportional to the normalized histogram of the discrete thickness map (6):

$$PS_{X, B, \Delta r(r_i)} = \frac{S}{\Delta r} h_{X_i}.$$

*Proof.* For $r_i \geq 0$,

$$PS_{X, B, \Delta r}(r_i) = - \frac{S(X \circ B(r_i)) - S(X \circ B(r_{i+1}))}{r_i - r_{i+1}}$$

$$= - \frac{\|X \circ B(r_i)\|_{L^1} - \|X \circ B(r_{i+1})\|_{L^1}}{r_i - r_{i+1}}$$

$$= \frac{\mu_{X, B}(r_i) - \mu_{X, B}(r_{i+1})}{\Delta r} = \frac{\|\chi_{X_i}(x, y)\|_{L^1}}{\Delta r}$$

$$= \frac{\iint \chi_{X_i}(x, y) dx dy}{S} \frac{S}{\Delta r} = \frac{S}{\Delta r} h_{X_i}.$$

For $r_i < 0$,

$$PS_{X, B, \Delta r}(r_i) = - \frac{S(X \bullet B(-r_i)) - S(X \bullet B(-r_{i+1}))}{r_{i+1} - r_i}$$

$$= \frac{\|X \bullet B(r_i)\|_{L^1} - \|X \bullet B(r_{i+1})\|_{L^1}}{r_{i+1} - r_i}$$

$$= \frac{\mu_{X, B}(r_i) - \mu_{X, B}(r_{i+1})}{\Delta r} = \frac{\|\chi_{X_i}(x, y)\|_{L^1}}{\Delta r}$$

$$= \frac{\iint \chi_{X_i}(x, y) dx dy}{S} \frac{S}{\Delta r} = \frac{S}{\Delta r} h_{X_i},$$

which was to be proven.

Define an EMD distance of type (3) between the morphological spectra of binary images of figures $X$ and $Y$:

$$d_{EMD\,PS}(PS_{X, B, \Delta r}, PS_{Y, B, \Delta r})$$

$$= \min_{\{h_{ij}\}} \sum_{j = -i_{max}}^{i_{max}} \sum_{i = -i_{max}}^{i_{max}} h_{ij} |r_i - r_j|;$$

$$h_{Y_j} = \frac{\Delta r}{S} PS_{Y, B, \Delta r}(r_j); \quad h_{X_i} = \frac{\Delta r}{S} PS_{X, B, \Delta r}(r_i); \quad (8)$$

$$d_E = |r_i - r_j|; \quad \sum_{j = -i_{max}}^{i_{max}} \sum_{i = -i_{max}}^{i_{max}} h_{ij} = 1,$$

$$\forall i, j: h_{ij} \geq 0; \quad h_{X_i} = \sum_{j = -i_{max}}^{i_{max}} h_{ij}; \quad h_{Y_j} = \sum_{i = -i_{max}}^{i_{max}} h_{ij}.$$

## TRUNCATED SPECTRA. INVARIANCE WITH RESPECT TO THE TRANSLATION AND ROTATION OF FIGURES

It is clear that, under translation (translation operator $\pi \in \Pi$) or rotation (rotation operator $\theta \in \Theta$) of figure $X$ within a frame ($\pi\theta X \subseteq K$), the positive part of the thickness map $t_{X, B, \Delta r}(r_i)$ and the corresponding
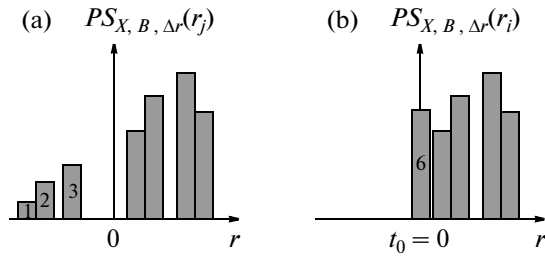
**Fig. 4.** Transition from a pattern spectrum to a lower truncated discrete spectrum: (a) discrete morphological spectrum and (b) lower truncated discrete morphological spectrum.



**Fig. 5.** Set of images of mythical creatures.

part of the morphological spectrum $PS_{X, B, \Delta r}(r_i)$ remain invariant:

$$t_{X, B, \Delta r}(x, y) = t_{\pi\theta X, B, \Delta r}(x, y);$$
$$t_{\pi\theta X, B, \Delta r}(x, y) \geq 0, \quad \pi\theta X \subset K;$$
$$PS_{X, B, \Delta r}(r_i) = PS_{\pi\theta X, B, \Delta r}(r_i); \quad (9)$$
$$r_i \geq 0, \quad \pi\theta X \subset K.$$

Define a discrete thickness map truncated from below,

$$T_{B, \Delta r, r0+}(f_X) = t_{X, B, \Delta r, r0+}(x, y)$$

$$= \begin{cases} t_{X, B, \Delta r}(x, y), & \text{if} \quad t_{X, B, \Delta r}(x, y) > r_0; \\ r_0, & \text{if} \quad t_{X, B, \Delta r}(x, y) \leq r_0 \end{cases} \quad (10)$$

and a discrete morphological spectrum truncated from below,

$$PS_{X, B, \Delta r, r0+}(r_i) = \begin{cases} PS_{X, B, \Delta r}(r_i), & \text{if} \quad r_i < r_0; \\ \sum_{j = -i_{\max}}^{r_0} PS_{X, B, \Delta r}(r_j), & \text{if} \quad r_i = r_0; (11) \\ 0, & \text{if} \quad r_i < r_0. \end{cases}$$

Figure 4 presents examples of a pattern spectrum and a discrete morphological spectrum truncated from below.

Consider $r_0 = 0$. Formula (9), as well as the fact that the area of the background is invariant under translations and rotations of a figure within a frame,

$$\{X \subseteq K, \pi\theta X \subseteq K\} \Rightarrow \|K \setminus \pi\theta X\|_{L^1} = \|K \setminus X\|_{L^1},$$

imply that the histograms of truncated thickness maps (truncated morphological spectra) are invariant under translations and rotations of figures within a frame:

$$PS_{X, B, \Delta r, 0+}(r_i) \equiv PS_{\pi\theta X, B, \Delta r, 0+}(r_i),$$
$$\pi\theta X \subset K. \quad (12)$$

Thus, truncated spectra without a negative part allow one to compare not only the images of figures, but also the shapes of figures that are invariant under translation and rotation. In practical applications, the truncation parameter can be chosen to be slightly
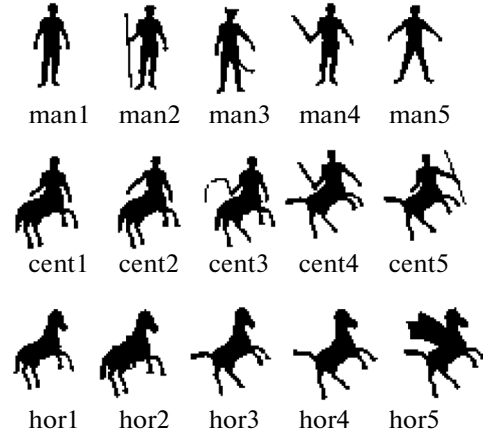
greater or less than zero, which either enriches or depletes the spectrum.

## EXPERIMENTS ON THE APPLICATION OF EMD-L[1] COMPARISON OF MORPHOLOGICAL SPECTRA IN THE PROBLEMS OF CLASSIFICATION OF IMAGES

In the first experiment, we considered a set of images [13] of mythical creatures: people, centaurs, and horses. Some of these figures were subjected to deformation within a class: either new objects were added to a figure, or the pose of an object was slightly changed within a class. Figure 5 presents examples of images from the set of mythical creatures.

The example shown in Fig. 6 illustrates the comparison of the morphological spectra of figures with the use of the EMD metric calculated with base distance $L^1$. One can see that the value of the EMD-L[1] distance between morphological spectra monotonically increases from the reference image of the figure of a human to the image of the figure of a centaur; in this metric, the closest images are those whose shapes are similar (for example, the silhouettes of a man without and with a spear).

On the basis of EMD-L[1] distances for all pairs of images within a set [13], the authors calculated the average intra-class and average inter-class distances for a set of images (Table 1). The calculated data show

**Table 1.** Average intra- and interclass EMD-L[1] distances for a set of images of mythical creatures

| Images | People | Centaurs | Horses |
|---|---|---|---|
| People | 0.812 | 3.054 | 6.31 |
| Centaurs | 3.054 | 0.69 | 2.25 |
| Horses | 6.31 | 2.25 | 0.78 |
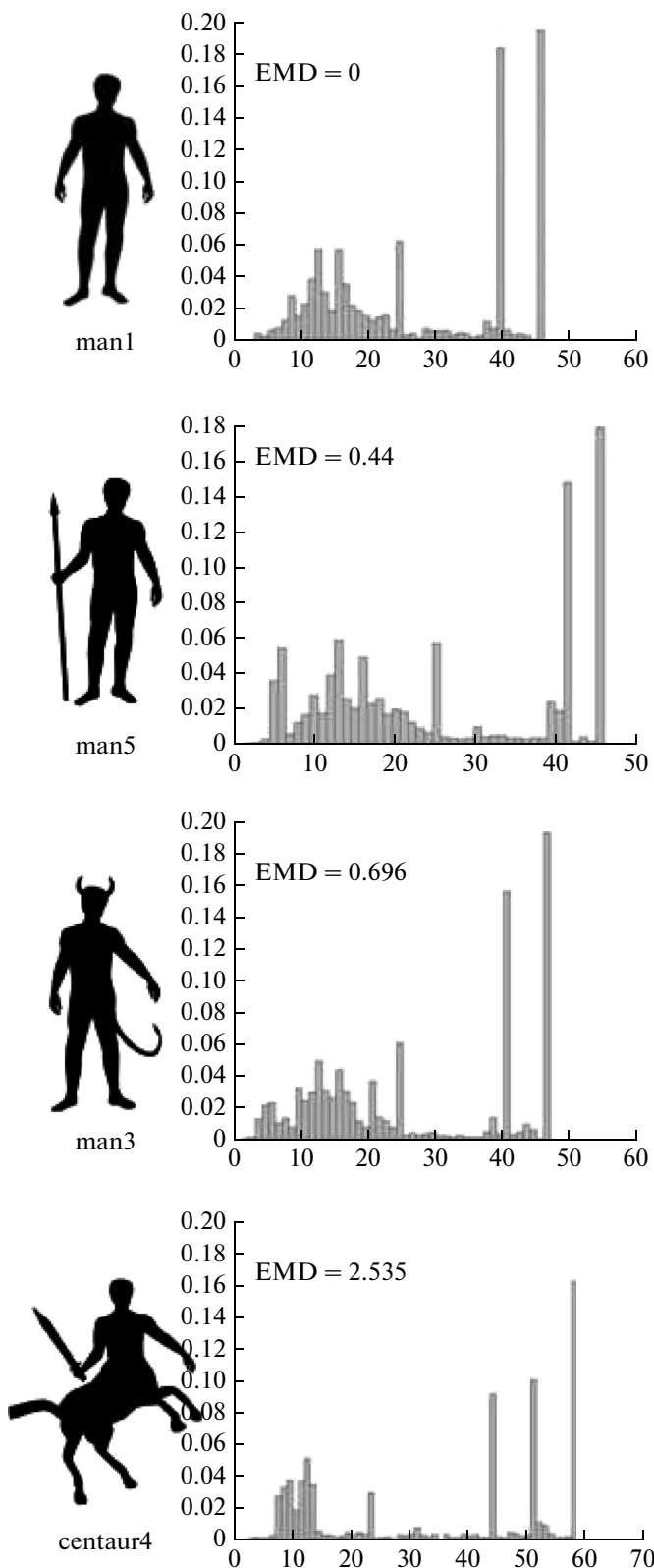
**Fig. 6.** Comparison of the morphological spectra of figures with the use of EMD metric calculated with base distance $L^1$; (a) EMD-$L^1$ = 0, (b) EMD-$L^1$ = 0.440, (c) EMD-$L^1$ = 0.696, and (d) EMD-$L^1$ = 2.535.
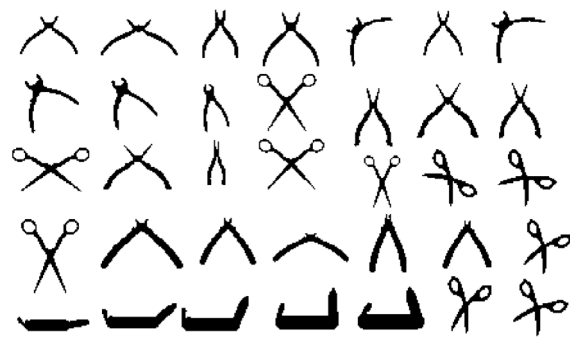


**Fig. 7.** Set of images of tools.

that the EMD-$L^1$ metric of comparison of the spectra of figures in this experiment well distinguishes objects of different classes: intraclass distances are substantially less than interclass distances. It is of interest that the figures of people are "far" from the figures of centaurs and horses; from the point of view of this metric, the centaurs are "closer" on average to the figure of a horse than to the figure of a human being. This result coincides with our intuitive perception of the similarity of such forms.

The second experiment was a so-called "experiment with queries" on a set of images [13] consisting of 36 images of figures of various tools (pliers, knives, and various types of scissors) (Fig. 7). For all binary images, we calculated discrete spectra (11) truncated at $r_0 = 0$, which we compared with the use of the EMD-$L^1$ metric (3').

Table 2 shows examples of such queries for a set of images of tools [13]. In all cases, we successfully found objects of the same type in a nearby location in the list of candidates arranged in the ascending order of distance, and the values of EMD-$L^1$ distance from a query to an object of the same type turned out to be much smaller than the distances to objects of other types presented in the database.

The experiments showed that a comparison of the morphological spectra with the use of EMD metric is an adequate way to compare figures, provided that the compared figures have sufficiently diverse distribution of thicknesses (spectrum). The EMD comparison turns out to be resistant to small deformations of flexible objects, to a change in their orientation in the plane, and to small noise on the boundaries of the figures.

The experiments were carried out on an Intel Core i5 PC operating at 3.0 GHz. The images of tools had a size of $635 \times 475$ pixels, and the images of mythical figures had a size of $530 \times 540$ pixels. The results shown in Table 3 confirm the computational efficiency of the approach.

For skeletization of images, we used a software library provided by L.M. Mestetsky [4]. The algorithms for constructing a morphological spectrum and

**Table 2.** EMD-L[1] closest images from the set of tools with respect to the interrogated image
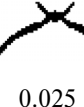
| Interrogated figure | | Five closest figures in the set of images of tools | | | | |
|---|---|---|---|---|---|---|
| EMD | 0 | 0.0226 | 0.025 | 0.0374 | 0.0379 | 0.094 |
| EMD | 0 | 0.01 | 0.012 | 0.023 | 0.037 | 0.27 |
| EMD | 0 | 0.037 | 0.059 | 0.062 | 0.093 | 0.5 |
| EMD | 0 | 0.012 | 0.013 | 0.014 | 0.021 | 0.15 |
| EMD | 0 | 0.03 | 0.044 | 0.065 | 0.77 | 0.52 |
| EMD | 0 | 0.02 | 0.025 | 0.026 | 0.027 | 0.1 |
| EMD | 0 | 0.01 | 0.018 | 0.0195 | 0.0198 | 0.363 |

**Table 3.** Average efficiency indices in milliseconds

| Set of images (the number of images in the dataset) | Average time of skeletization of one image, ms | Average time of constructing a morphological spectrum, ms | Average time of calculating EMD-L[1] distances when comparing spectra, ms | Total average time, ms |
|---|---|---|---|---|
| Tools (36) | 4.8 | 3.2 | <0.1 | 8 |
| Mythical creatures (15) | 6.8 | 15 | | 21.8 |

calculating EMD and EMD-L[1] distances were implemented by the authors of the present work. It is assumed that further software optimization will allow one to speed up the construction of morphological spectra. The current implementation of these spectra already ensures real-time processing of images with a rate of more than 25 frames per second. Thus, we have experimentally demonstrated that the EMD distance between spectra can be successfully used to solve the problems of shape classification of objects either as an additional feature or as the only feature (for images such as those shown in Figs. 5 and 7).

## CONCLUSIONS

In this paper, we have proposed a method for comparing discrete morphological spectra of binary images and plane figures with the use of the EMD

metric. We have introduced the concept of a thickness map of a binary image and proved the relation between the morphological pattern spectrum and the histogram of a thickness map. We have shown that truncated morphological spectra are invariant under the translation and rotation of figures. We have proposed a computationally efficient algorithm for comparing morphological spectra with the use of EMD metric with base distance $L^1$. We have demonstrated experimentally that the comparison of morphological spectra with the use of EMD-$L^1$ metric can be successfully applied to the problems of shape classification of objects.

## ACKNOWLEDGMENTS

## REFERENCES

1. P. Maragos, "Pattern spectrum and multiscale shape representation," IEEE Trans. Pattern Anal. Mach. Intellig. **11** (7), 701−716 (1989).

2. J. Serra, *Image Analysis and Mathematical Morphology* (Acad. Press, London, 1982).

3. Yu. V. Vizilter and S. V. Sidyakin, "The way to generate morphological semitone images," Vestn. Komp'yut. Inf. Tekhnol., No. 4, 8−17 (2012).

4. L. M. Mestetskii, *Continuous Morphology of Binary Images: Figures, Skeletons, Circulars* (Fizmatlit, Moscow, 2009) [in Russian].

5. A. Asano, "Texture analysis using morphological pattern spectrum and optimization of structuring elements," in *Proc. 10th Int. Conf. on Image Analysis and Processing (ICIAP'99)* (Venice, 1999), pp. 209−214.

6. A. Suruliandi and K. Ramar, "Local texture patterns − a univariate texture model for classification of images," in *Proc. 16th Int. Conf. "Advanced Computing and Communications" (ADCOM'08)* (Chennai, 2008), pp. 32−39.

7. Tchangou Toudjeu Ignace, *Pattern Spectra Algorithms for Pattern Recognition* (Tshwane University of Technology, 2006).

8. Y. Rubner, C. Tomasi, and L. J. Guibas, "The Earth mover's distance as a metric for image etrieval," Int. J. Comput. Vision, No. 40(2), 99−121 (2000).

9. S. S. Vallander, "The way to calculate Wasserstein distance between stochastic probabilities distribution in the strait line," Teor. Veroyatn. Ee Prim. **18** (4), 824−827 (1973).

10. S. T. Rachev, "Monge-Kantorovich problem on mass transport and its application in stochastics," Teor. Veroyatn. Ee Prim. **29** (4), 625−653 (1984).

11. E. I. Deza and M. M. Deza, *Distances Encyclopedia* (Nauka, Moscow, 2008) [in Russian].

12. Yu. P. Pyt'ev and A. I. Chulichkov, *Morphological Analysis Methods for Images* (Fizmatlit, Moscow, 2010) [in Russian].

13. A. M. Bronstein, M. M. Bronstein, A. M. Bruckstein, R. Kimmel, "Analysis of two-dimensional non-rigid shapes", Intl. Journal of Computer Vision (IJCV), Vol. 78/1, pp. 67−88, June 2008.

*Translated by I. Nikitin*



**Yurii V. Vizilter** was born in 1970. Graduated from Moscow Aviation Institute in 1992. Received his Candidate's Degree in Physics and Mathematics in 1997 and Doctoral Degree in 2009. Currently head of the Laboratory of Computer and Machine Vision at the State Research Institute of Aviation Systems. His scientific interests are processing and analysis of images, digital photogrammetry, machine vision, mathematical morphology, pattern recognition, machine learning, and biometry. Member of the editorial board of the journal *Vestnik komp'yuternykh i informatsionnykh tekhnologii* (Herald of Computer and Information Technologies). The author of more than 70 publications, of which 20 papers in peer-reviewed journals are in the list of the Higher Attestation Committee of the Russian Ministry of Education and Science.



**Sergei V. Sidyakin** was born in 1985. Graduated from Moscow Aviation Institute in 2009. Received his Candidate's Degree in 2013. Currently group head at the Division of Systems for Intelligent Data Analysis, Machine Vision, and Improved and Synthesized Vision at the State Research Institute of Aviation Systems. His scientific interests are image analysis and pattern recognition, machine vision, video surveillance, mathematical morphology, and pattern recognition. The author of 13 publications, including 8 papers.